Asymptotics of the Wigner 9*j*-symbol

2010 Class. Quantum Grav. 27 135010

(http://iopscience.iop.org/0264-9381/27/13/135010)

IOP PUBLISHING CLASSICAL AND QUANTUM GRAVITY

Class. Quantum Grav. **27** (2010) 135010 (17pp) doi:10.1088/0264-9381/27/13/135010

Asymptotics of the Wigner 9j-symbol

Hal M Haggard and Robert G Littlejohn

Department of Physics, University of California, Berkeley, CA 94720, USA

E-mail: robert@wigner.berkeley.edu

Received 29 December 2009, in final form 29 March 2010
Published 14 May 2010
Online at stacks.iop.org/CQG/27/135010

Abstract

We present the asymptotic formula for the Wigner 9j-symbol, valid when all quantum numbers are large, in the classically allowed region. As in the Ponzano–Regge formula for the 6j-symbol, the action is expressed in terms of lengths of edges and dihedral angles of a geometrical figure, but the angles require care in definition. Rules are presented for converting spin networks into the associated geometrical figures. The amplitude is expressed as the determinant of a 2×2 matrix of Poisson brackets. The 9j-symbol possesses caustics associated with the fold and elliptic and hyperbolic umbilic catastrophes. The asymptotic formula obeys the exact symmetries of the 9j-symbol.

PACS numbers: 03.65.Sq, 04.60.Pp, 02.20.Qs, 02.30.Ik

1. Introduction

The asymptotic behavior of spin networks has played a significant role in simplicial approaches to quantum gravity. Indeed, the field began with the observation that the Ponzano–Regge action (1968) for the semiclassical 6j-symbol is identical to the Einstein–Hilbert action of a tetrahedron in three-dimensional gravity in the Regge formulation (Regge (1961); see also Williams and Tuckey (1992) and Regge and Williams (2000)). More recently, semiclassical expansions have been used to study the low energy or classical limit of quantum gravity as well as to derive quantum corrections to the classical theory. Asymptotic studies in this area have included treatments of the 10j-symbol (Barrett and Williams 1999, Baez *et al* 2002, Barrett and Steele 2003, Freidel and Louapre 2003), amplitudes in the Freidel–Krasnov model (Conrady and Freidel 2008), LQG fusion coefficients (Alesci *et al* 2008) and the EPRL amplitude (Barrett *et al* 2009). In addition, the venerable 6j-symbol and Ponzano–Regge (1968) formula continue to receive attention (Roberts 1999, Barrett and Steele 2003, Freidel and Louapre 2003, Gurau 2008, Charles 2008, Littlejohn and Yu 2009, Dupuis and Livine 2009, Ragni *et al* 2010), not to mention the q-deformed 6j-symbol (Nomura 1989; Taylor and Woodward 2004, 2005).

In this paper we present the generalization of the Ponzano–Regge formula to the Wigner $9j$-symbol, as well as some material relevant for the asymptotics of arbitrary spin networks. The Ponzano–Regge formula (Ponzano and Regge 1968) gives the asymptotic expression for the Wigner $6j$-symbol when all quantum numbers are large. The $9j$-symbol is the next most complicated spin network after the $6j$-symbol, with features that are found in all higher spin networks. In this paper we present only the asymptotic formula itself for the $9j$-symbol and some salient facts surrounding it. We defer a derivation and deeper discussion of the formula to a subsequent publication.

Our derivation has quite a few steps, and some of them at this point are supported by numerical evidence only. Thus, we do not now have a rigorous derivation of our result. We believe it is correct, however, on the basis of direct numerical comparisons with the exact $9j$-symbol, the fact that our formula obeys all the symmetries of the exact $9j$-symbol, and the plausibility and numerical support for the conjectures involved in the parts of the derivation currently lacking proofs. The proofs do not seem difficult, and we hope to fill in the gaps in our future work.

Although most of the papers cited above have dealt with the asymptotics of specific spin networks, usually there are special values of the angular momenta that are used. For example, the $10j$-symbol involves balanced representations of $SO(4)$, which means that some pairs of j's are equal, while the $9j$-symbols that appear in LQG fusion coefficients have two columns in which one quantum number is the sum of the other two. In addition, j's are sometimes set equal because this is regarded as the most interesting regime from a physical standpoint.

As a result, the spin networks that have been studied tend to fall on caustics where the asymptotic behavior is not generic. At such points, the value of the spin network (the wavefunction) is not oscillatory in a simple sense, instead it has the form of a diffraction catastrophe (Berry 1976). In addition, the wavefunction scales as a higher (less negative) power of the scaling parameter (effectively, $1/\hbar$). This type of behavior has been noted in several places in the quantum gravity literature, although as far as we can tell no one has noted that it is related to standard caustic and catastrophe types. In this paper we give a rather complete picture of the $9j$-symbol for all possible parameters in the classically allowed region, including all phases and Maslov indices. We also indicate the subsets upon which the behavior is nongeneric and described by various types of caustics. We believe that this is the first time that such information has been available for any spin network more complicated than the $6j$-symbol.

Another reason for interest in the $9j$-symbol is that it is the nontrivial part of the Clebsch–Gordan coefficient for $SO(4)$.

Basic references on the Wigner $9j$-symbol include Edmonds (1960), Biedenharn and Louck (1981a, 1981b) and Varshalovich *et al* (1981). Recent work on the $9j$-symbol has included new asymptotic forms when some quantum numbers are large and others small (Anderson *et al* 2008, 2009). We also note the use of $SU(2)$ spin networks in quantum computing (Marzuoli and Rasetti 2005).

In section 2 we present the asymptotic formula for the $9j$-symbol and draw comparisons with the Ponzano–Regge formula to introduce its geometrical content. A detailed explanation of the notation follows in later sections. In section 3 we present general rules for converting spin networks into surfaces composed of oriented edges and oriented triangles, and illustrate them for the $9j$-symbol. In section 4 we explain how the geometrical objects (pieces of oriented surfaces) corresponding to the $9j$-symbol can be constructed in three-dimensional space. In section 5 we explain the configuration space of the $9j$-symbol and the classically allowed subset thereof. In section 6 we define the amplitude of the asymptotic formula and discuss the manifolds (the caustics) upon which it diverges as well as the diffraction

catastrophes that replace the simple asymptotic form in the neighborhood of the caustics. In section 7 we explain the phase of the semiclassical approximation, a generalization of the Ponzano–Regge action that requires careful definitions of dihedral angles. In section 8 we show that the asymptotic formula correctly obeys the symmetries of the $9j$-symbol. Finally, in section 9 we present some comments and conclusions.

2. The asymptotic formula

The asymptotic expression for the $9j$-symbol is

$$\begin{Bmatrix} j_1 & j_2 & j_3 \\ j_4 & j_5 & j_6 \\ j_7 & j_8 & j_9 \end{Bmatrix} = A_1 \cos S_1 + A_2 \sin S_2, \tag{1}$$

where $A_{1,2}$ are positive amplitudes, $S_{1,2}$ are phases and each term is roughly similar to the single term in the Ponzano–Regge formula for the $6j$-symbol. The right-hand side is the leading term in an asymptotic expansion in powers of $1/k$ of the $9j$-symbol when all nine j's are scaled by a positive factor k that is allowed to go to infinity (k plays the role of $1/\hbar$ in the asymptotic expansion). The k's are suppressed in (1), but the expression on the right-hand side scales as $1/k^3$. Equation (1) applies only in the classically allowed region. We do not present the analog of (1) in the classically forbidden region.

Equation (1) breaks down near caustics, where the $9j$-symbol scales with a higher (less negative) power of k than $1/k^3$. In the neighborhood of caustics, the $9j$-symbol is approximated by diffraction catastrophes, including the fold and hyperbolic and elliptic umbilic. These are discussed more fully in section 6.

To explain the meaning of (1) some analogies with the Ponzano–Regge formula for the $6j$-symbol are useful. In the classically allowed region, the Ponzano–Regge approximation is

$$\begin{Bmatrix} j_1 & j_2 & j_3 \\ j_4 & j_5 & j_6 \end{Bmatrix} = \frac{1}{\sqrt{2\pi\,|V_{123}|}} \cos\left(S + \frac{\pi}{4}\right), \tag{2}$$

where the phase and amplitude are expressed in terms of the geometry of a tetrahedron whose six edge lengths are $J_i = j_i + 1/2$. We let $\mathbf{J}_i$, $i = 1, \ldots, 6$, be classical vectors that run along the edges of the tetrahedron, such that $\mathbf{J}_3 + \mathbf{J}_4 + \mathbf{J}_5 = 0$, $\mathbf{J}_1 + \mathbf{J}_6 + \mathbf{J}_5$, $\mathbf{J}_3 = \mathbf{J}_1 + \mathbf{J}_2$ and $\mathbf{J}_6 = \mathbf{J}_2 + \mathbf{J}_4$. The amplitude is defined by $V_{123} = \mathbf{J}_1 \cdot (\mathbf{J}_2 \times \mathbf{J}_3)$, which is six times the volume of the tetrahedron, and the phase is defined by

$$S = \sum_{i=1}^{6} J_i \theta_i, \tag{3}$$

where θ_i is the exterior dihedral angle at edge i, that is, $\cos\theta_i$ is the dot product of the outward pointing normals of the two faces adjacent at edge i, such that $0 \leqslant \theta_i \leqslant \pi$.

More precisely, there are two tetrahedra associated with a $6j$-symbol, related by spatial inversion, that is, time-reversal. Except for flat configurations, the two tetrahedra are not related by proper rotations in $SO(3)$. We recall that time-reversal, not parity, inverts the direction of angular momentum vectors. The two tetrahedra correspond to the two stationary phase points of the $6j$-symbol, which make contributions to the asymptotic expression that are complex conjugates of each other. The result is the real cosine term in (2). One can say that semiclassically the $6j$-symbol is a superposition of two amplitudes, corresponding to a tetrahedral geometry and its time-reversed image, that produce oscillations in the result.

We shall use lower case j's for quantum numbers, and capital J's for the lengths of the corresponding classical vectors. These are always related by $J_i = j_i + 1/2$. The $1/2$ is a

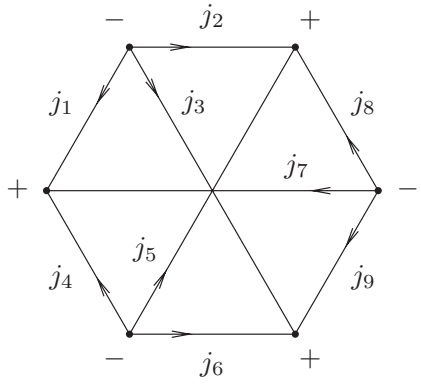

Figure 1. The spin network for the $9j$-symbol.

Maslov index (Maslov and Fedoriuk 1981, Mishchenko *et al* 1990, de Gosson 1997), and the manner in which it arises in this context is explained in Aquilanti *et al* (2007).

In the case of the $9j$-symbol in the classically allowed region, there are four geometrical figures associated with a given set of nine j's, consisting of two pairs related by time-reversal. The four geometrical figures correspond to the four real stationary phase points of the $9j$-symbol. Each pair of figures is associated with an 'admissible' root (defined momentarily) of a certain quartic equation. There are two admissible roots in the classically allowed region, labeled 1 and 2, corresponding to the two terms in (1). Each trigonometric term in (1) consists of an exponential and its complex conjugate, corresponding to a geometrical figure and its time-reversed image. One can say that semiclassically the $9j$-symbol is a superposition of four amplitudes corresponding to four geometries, consisting of two pairs of a geometry and its time-reversed image. We now explain these geometries and how they are specified by the nine j's that appear in the symbol.

3. Triangles, orientations and geometries

The $9j$-symbol specifies the lengths $J_i = j_i + 1/2$ of nine classical angular momentum vectors $\mathbf{J}_i$ but not their directions. Therefore, we inquire as to how the directions may be determined, and geometrical figures constructed out of the resulting vectors.

Actually, it is convenient to double this set and speak of 18 classical vectors $\mathbf{J}_i$, $\mathbf{J}'_i$, $i = 1, \ldots, 9$. A doubling of this kind was introduced by Roberts (1999), who gave a highly symmetrical way of writing the $6j$-symbol as a scalar product in a certain Hilbert space. Although Roberts only worked with the $6j$-symbol, his method is easily generalized to an arbitrary spin network. Ponzano and Regge (1968) also gave hints that doubling of angular momentum vectors is important in the asymptotic analysis of spin networks.

We now describe rules that take an arbitrary spin network (with at most trivalent vertices) and transcribe it into relations among a doubled set of classical angular momentum vectors, defining a set of oriented triangles and oriented edges of a geometrical figure. We exemplify these rules only in the case of the $9j$-symbol, but they are easily applied to any spin network. The reader may find it illuminating to apply our rules to the $6j$-symbol, starting with the usual spin network (the Mercedes graph). Figure 1 illustrates the spin network of the $9j$-symbol. See also figure 18.1 of Yutsis *et al* (1962).

Each edge of the spin network, labeled by j_i, is associated with two classical angular momentum vectors $\mathbf{J}_i$ and $\mathbf{J}'_i$ that are required to satisfy

$$|\mathbf{J}_i| = |\mathbf{J}'_i| = J_i = j_i + 1/2 \tag{4}$$

and

$$\mathbf{J}_i + \mathbf{J}'_i = 0. \tag{5}$$

Vectors $\mathbf{J}_i$ and $\mathbf{J}'_i$ have the same length and point in opposite directions.

Each vertex of the spin network, where three edges meet, corresponds to three vectors that add to zero. The three vectors are associated with the three edges. If the arrow on an edge ending at the vertex is pointing away from the vertex, then the angular momentum vector is unprimed; if it is pointing toward the vertex, then the vector is primed. This rule applied to figure 1 gives

$$\begin{aligned} &\mathbf{J}_1 + \mathbf{J}_2 + \mathbf{J}_3 = 0, \qquad &&\mathbf{J}'_1 + \mathbf{J}'_4 + \mathbf{J}'_7 = 0, \\ &\mathbf{J}_4 + \mathbf{J}_5 + \mathbf{J}_6 = 0, \qquad &&\mathbf{J}'_2 + \mathbf{J}'_5 + \mathbf{J}'_8 = 0, \\ &\mathbf{J}_7 + \mathbf{J}_8 + \mathbf{J}_9 = 0, \qquad &&\mathbf{J}'_3 + \mathbf{J}'_6 + \mathbf{J}'_9 = 0. \end{aligned} \tag{6}$$

These are a set of classical triangle relations, one for each vertex of the spin network. In the case of the $9j$-symbol, they are obviously related to the rows and columns of the symbol.

Although the vector addition in (6) is commutative, we agree to write the vectors in each equation in counterclockwise order (around the vertex of the spin network) for a vertex with + orientation, and in clockwise order for a vertex with − orientation, modulo cyclic permutations. Thus, the ordering of the vectors is the same as the ordering of the columns of the $3j$-symbol implied by the vertex of the network.

This ordering is used to define a set of oriented triangles. We take the three vectors of any one of equations (6) and place the base of one vector at the tip of the preceding one, to create the three edges of a triangle. In this process we parallel translate the vectors (in $\mathbb{R}^3$) but do not rotate them. The triangle is given an orientation (a definition of a normal) by taking the cross product of any two successive vectors defining the edges. For example, the normal to the 123-triangle is $\mathbf{J}_1 \times \mathbf{J}_2$, and that of the $1'4'7'$-triangle is $\mathbf{J}'_1 \times \mathbf{J}'_4$, which, in view of (5), is the same as $\mathbf{J}_1 \times \mathbf{J}_4$.

Next, we take the triangles and displace them so that the edge $\mathbf{J}_i$ of one triangle is adjacent to the edge $\mathbf{J}'_i$ of another triangle. In this process, the triangles are displaced but not rotated. If we do this with the six triangles defined by (6) in the case of the $9j$-symbol, we find that six pairs of edges can be made adjacent, as illustrated by the central six triangles of figure 2. In this 'central region' six pairs of vectors $\mathbf{J}_i$ and $\mathbf{J}'_i$ are adjacent for $i = 1, 2, 5, 6, 7, 9$. There is some arbitrariness in choosing which six pairs of edges will be made adjacent. If we wish that the remaining edges $i = 3, 4, 8$ also be paired, we can duplicate three of the triangles and attach them to the periphery of the central region, as illustrated in figure 2. This amounts to a kind of 'analytic continuation' of the central region.

Figure 2 is highly schematic. In general, the triangles are not equilateral, the surface that is formed by attaching them together is not planar, and the triangles may fold under one another.

The central region in figure 2 is a piece of an oriented surface, that is, all the normal vectors (by our convention) are pointing on the same side. In the case of the $6j$-symbol, our rules produce a closed surface (the usual tetrahedron), with normals all pointing either outward or inward (time-reversal converts one into the other). In the case of the $9j$-symbol, the surface is not closed. There is some suggestion that this surface represents a triangulation of $\mathbb{R}P^2$ but for this paper we shall view it as living in $\mathbb{R}^3$.

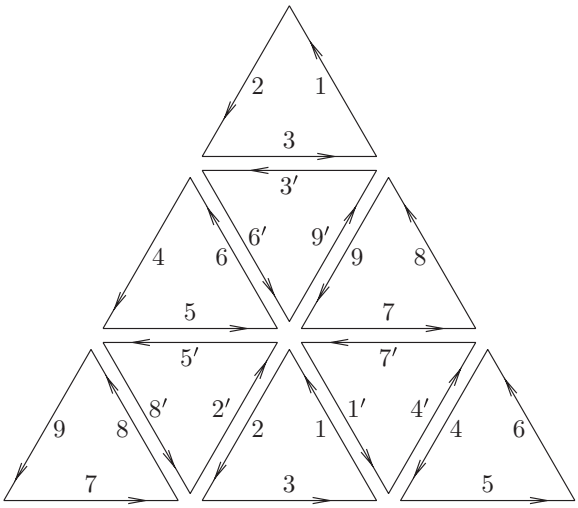

Figure 2. The six triangles defined by (6) form the 'central region' of the figure, with three triangles duplicated and attached to the edges of the central region. The notation 1, 2′, etc refers to $\mathbf{J}_1, \mathbf{J}_2'$, etc.

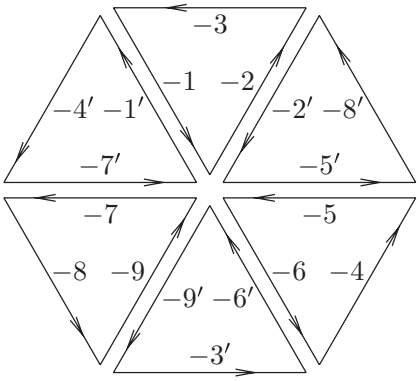

Figure 3. The central region of the time-reversed surface. Notation -1, $-2'$, etc refers to $-\mathbf{J}_1$, $-\mathbf{J}_2'$, etc.

Finally, we orient each edge by choosing the direction of the vector $\mathbf{J}_i$ (not $\mathbf{J}_i'$).

We will be interested in finding solutions $\{\mathbf{J}_i, \mathbf{J}_i', i = 1, \ldots, 9\}$ of (4)–(6), modulo overall proper rotations (in $SO(3)$). That is, although we do not rotate vectors or faces when forming our surface with oriented faces and edges, we are allowed to rotate the whole surface once completed.

We note that if $\{\mathbf{J}_i, \mathbf{J}_i', i = 1, \ldots, 9\}$ is a solution of these equations, then the time-reversed set $\{-\mathbf{J}_i, -\mathbf{J}_i', i = 1, \ldots, 9\}$ is also a solution. If we apply our rules for converting vectors into a surface, we will find in general that the time-reversed set produces a different surface (not equivalent under $SO(3)$). We apply time-reversal only to the vectors, not the rules; for example, the ordering of the time-reversed vectors is the same as the original vectors. The central six triangles of the time-reversed surface are illustrated in figure 3.

To visualize the surfaces in figures 2 and 3, we may imagine that the central region of figure 2 bulges out of the paper, like the northern hemisphere of a sphere (whether it does or not depends on the parameters, but this is one possibility). Then the time-reversed surface in figure 3 bulges into the paper, since spatial inversion is equivalent, modulo $SO(3)$, to reflection in a plane. Then the central region of figure 2 can be glued to the time-reversed surface in figure 3, bringing edge $\mathbf{J}_3'$ adjacent to edge $-\mathbf{J}_3$, etc, and producing a surface homeomorphic to S^2. This is the hexagonal bipyramid constructed by Ponzano and Regge (1968). The conventional normals are pointing outward in the northern hemisphere, and inward on the southern. As noted by Ponzano and Regge, this bipyramid is bisected by three planes passing through a common line, namely the 'axis' of the sphere, which cut the bipyramid into three pairs of congruent tetrahedra. These correspond to the three $6j$-symbols in the representation of the $9j$-symbol as a sum over products of $6j$-symbols (see Edmonds (1960) equation (6.4.3)), in which the variable of summation is the common edge of the tetrahedra (the axis of the sphere).

4. Finding the vectors

To find a solution of (4)–(6) we note that all 18 vectors are determined if only four of them, $\{\mathbf{J}_1, \mathbf{J}_2, \mathbf{J}_4, \mathbf{J}_5\}$, are given. We let G be the 4×4 Gram matrix constructed out of these vectors, that is, the 4×4, real symmetric matrix of dot products of these vectors among themselves. Of the ten independent dot products, eight can be determined from the given lengths J_i, $i = 1, \ldots, 9$. That is, the diagonal elements are J_i^2, $i = 1, 2, 4, 5$, while

$$\begin{aligned} \mathbf{J}_1 \cdot \mathbf{J}_2 &= \left(J_3^2 - J_1^2 - J_2^2\right)/2, \qquad & \mathbf{J}_1 \cdot \mathbf{J}_4 &= \left(J_7^2 - J_1^2 - J_4^2\right)/2, \\ \mathbf{J}_2 \cdot \mathbf{J}_5 &= \left(J_8^2 - J_2^2 - J_5^2\right)/2, \qquad & \mathbf{J}_4 \cdot \mathbf{J}_5 &= \left(J_6^2 - J_4^2 - J_5^2\right)/2. \end{aligned} \tag{7}$$

The two dot products that cannot be determined from the given lengths are $u = \mathbf{J}_1 \cdot \mathbf{J}_5$ and $v = \mathbf{J}_2 \cdot \mathbf{J}_4$, which we regard as unknowns. These satisfy a linear equation obtained by squaring $\mathbf{J}_9 = -\mathbf{J}_3 - \mathbf{J}_6$:

$$J_9^2 = J_3^2 + J_6^2 + 2(u + v + \mathbf{J}_1 \cdot \mathbf{J}_4 + \mathbf{J}_2 \cdot \mathbf{J}_5). \tag{8}$$

Another equation connecting u and v is $\det G = 0$, which holds since the four vectors lie in $\mathbb{R}^3$ and the 4-simplex defined by them is flat. This is a quartic equation in u and v, which by using (8) to eliminate v can be converted into a quartic equation in u alone. We write this quartic as $Q(u) = 0$. We find the roots u of this quartic, solve for v by using (8), whereupon all components of the Gram matrix become known (there is one Gram matrix for each root).

Ponzano and Regge (1968) discussed this procedure in somewhat different language, and apparently believed that all four roots would contribute to the asymptotics of the $9j$-symbol. In fact, they do, if one wishes to work in the classically forbidden region and/or take into account tunneling and exponentially small corrections in the neighborhood of internal caustic points (more about these below). But in the classically allowed region the asymptotics of the $9j$-symbol are dominated by the contributions from 'admissible' roots, namely, those roots that produce Gram matrices that can be realized as dot products of real vectors $\mathbf{J}_i$. Only these correspond to real geometrical figures of the type we have described.

If a root u of $Q(u) = 0$ is complex, then it produces a complex Gram matrix that cannot be realized with real vectors, and so u is inadmissible. But a real Gram matrix can be realized as the dot products of real vectors if and only if it is positive semidefinite; so even if u is real it will still be inadmissible if G has negative eigenvalues.

We define the classically allowed region of the $9j$-symbol as the region in which $Q(u)$ has at least one admissible root. In fact, in the classically allowed region $Q(u)$ has four real

roots of which two are generically admissible. We order the four real roots of $Q(u)$ in the classically allowed region in ascending order and label them by $k = 0, 1, 2, 3$. It turns out that the two admissible roots are the middle two, $k = 1, 2$, corresponding to the two terms of (1) with the same subscripts, $k = 1, 2$.

For a given admissible root, that is, a positive semidefinite Gram matrix, we wish to find the vectors $\mathbf{J}_i$, $i = 1, 2, 4, 5$. We arrange the four unknown vectors as the columns of a 3×4 matrix F, so that $G = F^T F$. To find F given G, we diagonalize G, $G = VKV^T$, where $V \in O(4)$ and K is diagonal with nonnegative diagonal entries (the eigenvalues of G). At least one of these eigenvalues must be 0; we place it last, and write $K = D^T D$, where D is a real, 3×4 diagonal matrix. Then $F = UDV^T$, where U is an arbitrary element of $O(3)$. This generates all possible sets of vectors whose dot products are realized in G; it amounts to using the singular value decomposition of F. If $U = R \in SO(3)$ then we generate a set of surfaces related by overall rotations; if $U = -R$ we generate the time-reversed set. In this way a single Gram matrix, corresponding to a single admissible root of the quartic, produces a geometry and its time-reversed image. Altogether, the two admissible roots imply the four geometries in (1).

This method of finding F is discussed in the context of the $6j$-symbol by Littlejohn and Yu (2009), where it is also applied in the classically forbidden region. There we find complex angular momentum vectors that satisfy the required algebraic relations. This carries over to the $9j$-symbol in the classically forbidden region. In the literature on the $6j$-symbol it is common to state that a Euclidean group applies in the classically allowed region and a Lorentz group in the classically forbidden region; but for the $9j$-symbol the groups are actually $SO(3, \mathbb{R})$ and $SO(3, \mathbb{C})$.

5. The classically allowed region and configuration space

The classically allowed region is a subset of full dimensionality of the nine-dimensional parameter space of the $9j$-symbol, itself a convex subset of $\mathbb{R}^9$ defined by the triangle inequalities. To visualize this and other subsets of the parameter space it helps to fix seven of the j's to obtain a two-dimensional slice. Figure 4 illustrates such a slice for the case

$$\begin{Bmatrix} 129/2 & 137/2 & j_3 \\ 113/2 & 121/2 & j_6 \\ 64 & 108 & 90 \end{Bmatrix}, \tag{9}$$

in which only j_3 and j_6 are allowed to vary. The choice of j_3 and j_6 for this purpose is not arbitrary, since these two j's are quantum numbers for a pair of commuting operators on a space of 5-valent $SU(2)$ intertwiners. They are like x and y for a wavefunction $\psi(x, y)$. In this analogy, we think of (j_3, j_6)-space as a 'configuration space' for the $9j$-symbol and the $9j$-symbol itself as a 'wavefunction' $\psi(j_3, j_6)$. We will mostly use the variables $J_3 = j_3 + 1/2$, $J_6 = j_6 + 1/2$ to describe this space. When thinking in classical terms, J_3 and J_6 are continuous variables (not quantized).

Figure 4 illustrates a convex region of the J_3–J_6 plane, bounded by straight lines and defined by the classical triangle inequalities:

$$\begin{aligned} &\max(|J_1 - J_2|, |J_6 - J_9|) \leqslant J_3 \leqslant \min(J_1 + J_2, J_6 + J_9), \\ &\max(|J_4 - J_5|, |J_3 - J_9|) \leqslant J_6 \leqslant \min(J_4 + J_5, J_3 + J_9). \end{aligned} \tag{10}$$

Properly speaking, configuration space is this convex region, not the whole plane. The unshaded area inside the convex region is the classically allowed region, surrounded by the shaded classically forbidden region. The caustic curve separates the classically allowed from

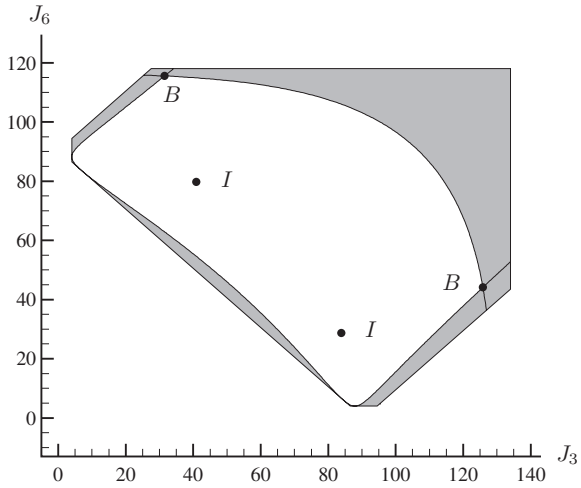

Figure 4. The convex region of the J_3–J_6 plane is the configuration space of the $9j$-symbol. The shaded area is the classically forbidden region, and the unshaded, the classically allowed. Points I are internal caustics, two of the flat configurations; points B are the other two flat configurations, lying on the boundary curve.

the classically forbidden regions; it has kinks (discontinuities in slope) at points B, and is tangent to the boundary of the convex region at several points. Other features of this figure are explained below.

Given a point (J_3, J_6) of the classically allowed region, the procedure described in sections 3 and 4 produces a quartic polynomial $Q(u)$ whose two middle roots $k = 1, 2$ are admissible. These can be thought of as specifying a two-branched 'root surface' that sits over the classically allowed region. The two middle roots coalesce as we approach the caustic curve, and become (inadmissible) complex conjugates as we move beyond. Thus, the two root surfaces can be thought of as being glued together on the caustic curve.

Corresponding to each root there are two geometries modulo $SO(3)$, related by time-reversal, so there is a two-fold 'geometry surface' sitting above each root surface, or four geometry surfaces sitting above the classically allowed region. These four geometry surfaces are actually branches of the projection of an invariant 2-torus onto configuration space, and correspond to the four exponential terms in (1). This 2-torus sits in the phase space of the $9j$-symbol, a four-dimensional, compact symplectic manifold.

This symplectic manifold is only one of several phase spaces that describe the classical mechanics of the $9j$-symbol, but all the others have higher dimensionality so we call this one the 'phase space of minimum dimensionality.' It is one of the symplectic manifolds discovered by Kapovich and Millson (1996). Its analog in the case of the $6j$-symbol is a spherical phase space, which has been studied by Charles (2008) and by Littlejohn and Yu (2009). The phase space of minimum dimensionality is related to other phase spaces for the $9j$-symbol by a combination of symplectic reduction (Marsden and Ratiu 1999) and the elimination of constraints. We have found it useful to employ all these spaces in our work on the $9j$-symbol.

6. The amplitude and caustics

The amplitudes of semiclassical approximations are notorious for the computational difficulties they cause. For example, several authors have resorted to computer algebra and/or numerical

experimentation to check the amplitude determinant in the Ponzano–Regge formula. Actually, this amplitude (due originally to Wigner (1959)) is given by a single Poisson bracket between intermediate angular momenta (Aquilanti *et al* 2007, and, in more detail, Littlejohn and Yu 2009), which can be evaluated in a single line of algebra. More generally, semiclassical amplitudes are easily found in terms of matrices of Poisson brackets.

In the case of the $9j$-symbol we define

$$V_{ijk} = \mathbf{J}_i \cdot (\mathbf{J}_j \times \mathbf{J}_k), \tag{11}$$

which is six times the signed volume of the tetrahedron specified by edges i, j, k (it is the volume of the corresponding parallelepiped). Then the amplitudes A_1, A_2 in (1) are given by

$$A = \frac{1}{4\pi\sqrt{|\det D|}}, \tag{12}$$

where

$$D = \begin{pmatrix} V_{124} & V_{215} \\ V_{451} & V_{542} \end{pmatrix}. \tag{13}$$

The subscripts 1,2 are omitted on A in (12) because the same formula applies for both terms in (1), but $A_1 \neq A_2$ in general because the formula is evaluated on two different geometries (associated with the two admissible roots). The quantity $\det D$ is even under time-reversal, so the same amplitude applies to both a geometry and its time-reversed image.

The volumes in matrix D are Poisson brackets of intermediate angular momenta in a recoupling scheme for the $9j$-symbol, which are most easily evaluated in the phase space of minimum dimensionality. We omit details; suffice it to say for now that the derivation of matrix (13) in terms of Poisson brackets and thence the amplitude is extremely easy.

We define the caustic set as the subset of the $9j$-parameter space where $\det D = 0$. Its intersection with the two-dimensional slice seen in figure 4 consists of the union of the caustic curve (the curve separating the classically allowed from the classically forbidden region) with the two points marked I. In addition, the caustic set includes the continuation of the caustic curves from points B into the classically forbidden region. The points I are 'internal' caustics, that is, internal to the classically allowed region. While the caustic curve has codimension 1, the internal caustics have codimension 2.

The quantity $\det D$ is nonzero away from the caustics. It turns out that the sign of $\det D$ distinguishes the two root surfaces, with $\det D > 0$ on root surface 1 and $\det D < 0$ on root surface 2.

The caustics of the $6j$-symbol occur at the flat configurations (flat tetrahedra), as appreciated by Ponzano and Regge (1968) and Schulten and Gordon (1975a, 1975b). The caustics of the $9j$-symbol, however, are not in general flat, that is, $\det D = 0$ does not imply that the configuration is flat. The flat configurations of the $9j$-symbol, however, do lie on the caustic set. In a given J_3–J_6 slice, there are precisely four flat configurations. In the example of figure 4, these are marked B and I. The points B are flat configurations lying on the boundary of the classically allowed region (the caustic curve), while points I are internal flat configurations. As we vary the seven j's that are fixed in figure 4, the number of flat configurations on the boundary varies from 2 to 4; those not on the boundary are internal.

In the usual manner of semiclassical approximations, (1) breaks down in a neighborhood of the caustic set (it diverges exactly at the caustic), and must be replaced by a diffraction function associated with a catastrophe (Berry 1976). In the case of the $6j$-symbol, the only catastrophe that occurs is the fold, yielding an Airy function as the semiclassical approximation, as noted by Ponzano and Regge (1968) and Schulten and Gordon (1975). This is the normal situation for systems of one degree of freedom. The $9j$-symbol, however, possesses two degrees of

freedom, and other types of catastrophes occur. The fold catastrophe applies at most points along the caustic curve, where the $9j$-symbol is approximated by an Airy function; but at flat configurations there is an umbilic catastrophe, hyperbolic for those (B) falling on the boundary (caustic) curve and elliptic for the internal caustics (I). See Trinkhaus and Drepper (1977) for illustrations of the associated diffraction functions. The umbilic catastrophes are generic in systems of three degrees of freedom but occur in the $9j$-symbol (with only two) because of time-reversal symmetry. However, only sections of the full three-dimensional umbilic wave forms appear (Berry 1976). The cusp catastrophe, which can be expected in generic systems of two degrees of freedom, does not occur in the classically allowed region of the $9j$-symbol.

Caustics are associated with the coalescence of branches of the projection of a Lagrangian manifold in phase space onto configuration space. In the case of the $9j$-symbol, the Lagrangian manifold is the invariant 2-torus mentioned in section 5. Along the boundary of the classically allowed region, the two admissible roots coalesce, which means that the four geometries merge into two. At most points on the boundary curve, the two remaining geometries are not equal, but are related by time-reversal. At such points we have a fold catastrophe, and the $9j$-symbol is approximated by an Airy function (modulated by a cosine term). At points B, however, the two geometries related by time-reversal merge into a single flat configuration, producing the hyperbolic umbilic catastrophe.

At internal caustic points I the geometry and its time-reversed image for one of the two admissible roots coalesce to produce a flat configuration. The two geometries of the other root surface, however, do not coalesce. Thus, at internal caustics I there are three geometries. Only the flat configuration associated with one of the roots produces the elliptic umbilic catastrophe; thus, only one of the two terms in (1) is replaced by the elliptic umbilic diffraction function, while the other remains as shown in (1). The $9j$-symbol is a linear combination of these two terms, but the elliptic umbilic diffraction function dominates when the scaling factor k is large.

The caustics have a certain size, that is, a distance around the caustic set over which diffraction functions must be used instead of (1). This distance Δj scales as $k^{1/3}$ for all three catastrophe types (fold and elliptic and hyperbolic umbilic) discussed here.

In the neighborhood of fold catastrophes the wavefunction scales as $k^{-17/6}$, that is, $k^{1/6}$ higher than the k^{-3} of the two terms in (1). In the neighborhood of umbilic catastrophes the scaling is $k^{-8/3}$, that is, with another factor of $k^{1/6}$. For large values of k the $9j$-symbol is largest near the points I, B.

Linear combinations with different scaling behaviors have been observed by Barrett and Steele (2003) and by Freidel and Louapre (2003) in their studies of the $10j$-symbol. It seems that the $9j$-symbol is the simplest spin network in which this phenomenon occurs.

7. The phase

The phases S_1 and S_2 in (1) each have the form

$$S = \sum_{i=1}^{9} J_i \theta_i, \tag{14}$$

where θ_i is the angle between normals of adjacent faces of the geometrical figure. This of course is similar to the Ponzano–Regge formula, but the $6j$-tetrahedron is convex and all dihedral angles can be taken in the interval $[0, \pi]$. The dihedral angles for the $9j$-symbol, on the other hand, must be allowed to lie in a full 2π interval, as explained momentarily. The subscripts 1,2 are omitted on S in (14) because the same formula applies to both terms in (1). The formula must be evaluated, however, on two different geometries, so S_1 and S_2 are not equal. In addition, the angles θ_i lie in different intervals for the two geometries.

Each edge i of the geometrical figure is adjacent to two faces, for example, edge 4 in figure 2 is adjacent to faces $1'4'7'$ and 456. One face adjacent to edge i contains vector $\mathbf{J}_i$, and the other $\mathbf{J}'_i$. Let the two normals of these two faces, according to the conventions given above, be $\hat{\mathbf{n}}$ and $\hat{\mathbf{n}}'$. Then we define θ_i as the angle such that

$$R(\hat{\boldsymbol{\jmath}}, \theta_i)\hat{\mathbf{n}} = \hat{\mathbf{n}}', \tag{15}$$

where $\hat{\boldsymbol{\jmath}}$ is the unit vector along $\mathbf{J}$, specifying the axis of a rotation R by angle θ_i using the right-hand rule. In the Ponzano–Regge formula one can compute the dihedral angle from its cosine, but for the $9j$ one must also use the sine of the angle. That is, (15) is equivalent to

$$\hat{\mathbf{n}}' = \cos\theta_i\, \hat{\mathbf{n}} + \sin\theta_i\, \hat{\boldsymbol{\jmath}} \times \hat{\mathbf{n}}. \tag{16}$$

This determines θ_i to within an additive integer multiple of 2π. We add the further requirement that for the geometries associated with the first root (the cosine term in (1)), $-\pi \leqslant \theta_i < +\pi$, while for the second root (the sine term in (1)), $0 \leqslant \theta_i < 2\pi$. These ranges for the angle θ_i are chosen because they give a continuous branch for the angle over the two root surfaces. It turns out that θ_i never crosses $\pm\pi$ on the surface for root 1, and it never crosses 0 or 2π on the surface for root 2.

The rules given in sections 3 and 4 for converting vectors into surfaces with oriented edges and triangles are an essential part of the definition of the dihedral angles θ_i. It is of interest to see how the angles change when a set of vectors or the associated geometry is subjected to some symmetry.

Under time-reversal, the orientation of all triangles reverses, that is, the normal vectors stay the same but the vectors defining the edges are inverted. This means that the angles θ_i go into $-\theta_i$ on root surface 1, while they go into $2\pi - \theta_i$ on root surface 2 (both changes guarantee that the angles remain within their respective ranges). Thus, S goes into $-S$ on root surface 1 and

$$S \to -S + 2\pi\nu + 9\pi \tag{17}$$

on root surface 2, where ν is the integer

$$\nu = \sum_{i=1}^{9} j_i. \tag{18}$$

These guarantee that $\cos S_1$ and $\sin S_2$ are invariant under time-reversal. Since the same applies to the amplitudes A_1 and A_2, one can choose either a geometry or its time-reversed image, for each root, when evaluating (1).

This completes the definition and geometrical interpretation of all the notation used in (1).

8. Symmetries of the $9j$-symbol

Formula (1) transforms correctly under the symmetries of the $9j$-symbol (Varshalovich *et al* 1981, section 10.4), which state that the $9j$-symbol suffers a phase change of $(-1)^\nu$ under odd permutations of rows or columns or under transposition. Consider, for example, the swapping of the first two columns, and let P be the permutation of indices, so that $P1 = 2$, $P2 = 1$, $P3 = 3$, etc. This maps an old set of nine j's into a new set, and old quartic $Q(u) = 0$ into a new one, etc. We find that the u root of the old quartic becomes the v root of the new one, which amounts to saying that the root 1 surface of the old geometry is mapped into the root 2 surface of the new one, and vice versa. Also, the orientations of the three unprimed triangles reverse, but not those of the primed ones, causing all nine dihedral angles to be incremented

or decremented by π (depending on the range). If we let θ_i be the original angles and $\tilde{\theta}_i$ the new ones, then when θ_i is on root surface 1 we find $\tilde{\theta}_{Pi} = \theta_i + \pi$, which means that the new angle is in the right range since it is on root surface 2. Similarly, when θ_i is on root surface 2 then $\tilde{\theta}_{Pi} = \theta_i - \pi$, which is in the right range since $\tilde{\theta}_{Pi}$ is on root surface 1. As a result, when the original geometry is on root surface 1, we have

$$\sum_{i=1}^{9} J_i \tilde{\theta}_i = \sum_{i=1}^{9} J_i \theta_i + \nu\pi + \frac{9\pi}{2}, \tag{19}$$

so that $\sin \tilde{S}_2 = (-1)^\nu \cos S_1$, while if the original geometry is on root surface 2, we have

$$\sum_{i=1}^{9} J_i \tilde{\theta}_i = \sum_{i=1}^{9} J_i \theta_i - \nu\pi - \frac{9\pi}{2}, \tag{20}$$

so that $\cos \tilde{S}_1 = (-1)^\nu \sin S_2$. The sine and cosine terms in (1) swap under column swap, and the result acquires an overall phase of $(-1)^\nu$, as required. The specified ranges on the dihedral angles on the two root surfaces are necessary for this to work out.

9. Comments and conclusions

It is easy to derive expression (14) by the method of Roberts (1999), which involves rotating faces by an angle of π about their normals, and edges by an angle of π about a normal to them. The phase (14) (times 2) is then an action integral along one Lagrangian manifold and back along another (the analogs of the A- and B-manifolds of Aquilanti *et al* (2007)). Similar expressions apply to any spin network of any complexity. But the contours chosen for the integration are not unique, in that one can add any multiples of quantized loops on the two manifolds. These modify both the actions and the Maslov indices, and amount to changing the choice of branch for the angles θ_i, that is, adding an integer multiple of 2π to these angles. This does not leave the trigonometric functions in (1) invariant because the angles are multiplied by the J_i, which may be half-integers. The result is that the phase of the approximation to the $9j$-symbol depends on the contours. A more serious worry is that the contours, that is, the branches for the θ_i, may change as we move around in the parameter space of the $9j$-symbol. This would amount to crossing a branch cut for the angles θ_i (and there are different branch cuts for different angles). In addition, as we move around in parameter space we can make any two adjacent faces rotate relative to one another around their common edge as many times as we want. Although the phases in question are 'only' powers of -1, straightening out this issue was by far the hardest part of this work. In the end we realized that the ranges $[-\pi, +\pi)$ on root surface 1 and $[0, 2\pi)$ on root surface 2 guarantee that there are no branch cuts and hence no discontinuities. The ranges specified for the angles θ_i give us in effect a global, smooth definition of contours for carrying out action integrals.

We present several numerical comparisons of (1) with the exact $9j$-symbol. In figure 5 approximation (1) (smooth curve) may be compared to the exact $9j$-symbol (sticks) as a function of j_3 for fixed values of the other j's. The range chosen lies inside the classically allowed region, far from a caustic. Figure 6 shows the comparison in a range that crosses a fold catastrophe, and figure 7 shows the comparison in an interval that passes near a hyperbolic umbilic catastrophe (the upper point I in figure 4). Approximation (1) is too large near the point I.

Varshalovich *et al* (1981) present an asymptotic approximation for the $9j$-symbol without citation (their equation (10.7.1)), which is different from our formula (1). In figure 8 we

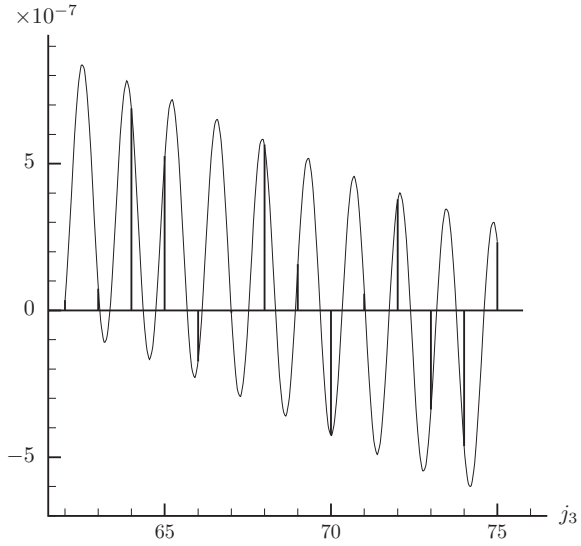

Figure 5. Comparison of exact $9j$-symbol (vertical sticks) with approximation (1), away from a caustic. Values used are those in (9), with $j_6 = 50$.

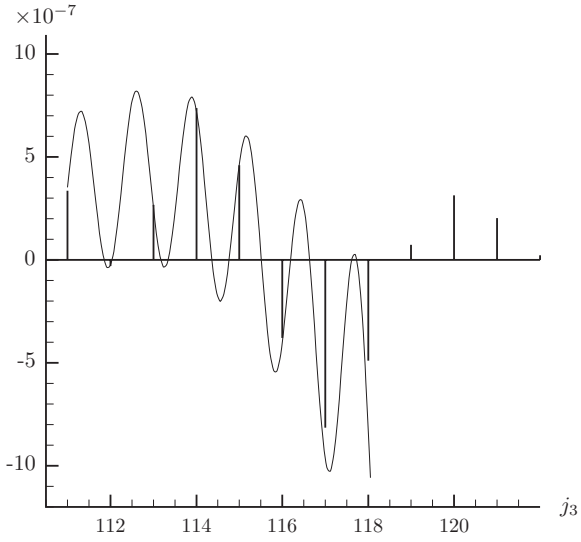

Figure 6. Like figure 5, but an interval that spans a fold catastrophe (with $j_6 = 60$). Approximation (1) is discontinued at the caustic, the exact values are continued into the classically forbidden region.

compare the exact $9j$-symbol with the formula of Varshalovich *et al* and with our formula (1), for the values

$$\begin{Bmatrix} 32 & 34 & j_3 \\ 28 & 61/2 & 81/2 \\ 26 & 73/2 & 91/2 \end{Bmatrix}. \tag{21}$$

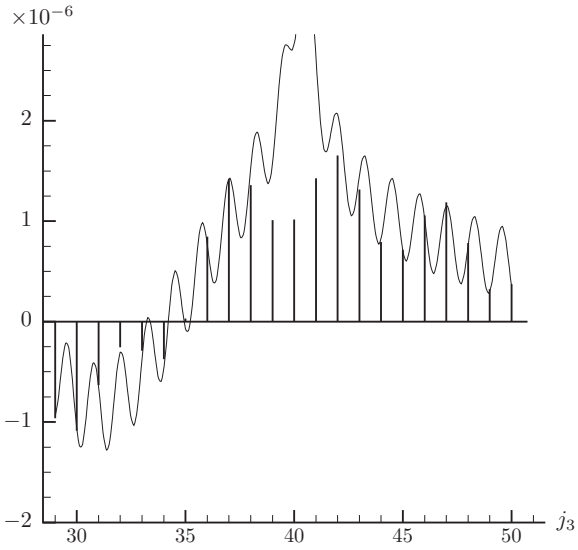

Figure 7. Like figure 6, but passing near an ellipitc umbilic catastrophe (with $j_6 = 79$).

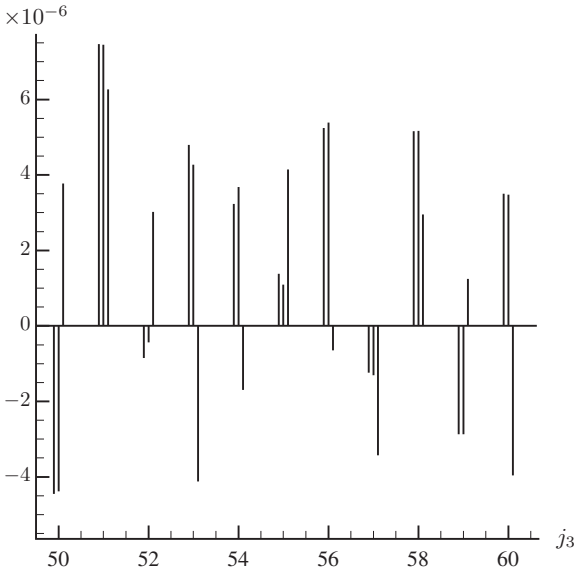

Figure 8. Near each quantized value of j_3, there are three lines. The other eight j's are given by (21). The left line is the exact $9j$-symbol, the middle line is approximation (1), and the right is formula (10.7.1) of Varshalovich *et al* (1981).

The formula of Varshalovich *et al* vanishes at many places inside the classically allowed region, as we have defined it, so it takes some searching to find an interval where both their formula and ours give nonzero results. On the basis of such comparisons, we believe that the formula of Varshalovich *et al* is an asymptotic result in a different sense than ours, or else it is incorrect.

The two terms in (1) have different trigonometric functions (sine and cosine) because there is a relative Maslov index of 2 between the two root surfaces. The relative Maslov index between a geometry and its time-reversed image is 0, a somewhat surprising result because in mechanical systems and in the $6j$-symbol the Maslov index between a branch or geometry and its time-reversed image is 1.

When an interior caustic occurs on a root surface, the two geometries that sit above it form a double cover, in the manner of the Riemann sheet for the square root function. The internal caustic point I is a branch point for the cover. Geometries transform continuously into their time-reversed images as we go around the point I, without crossing a caustic.

Several studies of the asymptotics of spin networks have started with an integral representation of the network, to which the stationary phase approximation is applied. Roberts (1999) represented the $6j$-symbol as a scalar product in a certain Hilbert space, which was put into the coherent state representation, whereupon the integral was evaluated by the stationary phase approximation. Coherent states have played a prominent role in many recent semiclassical studies. Our approach has been to work as much as possible in a representation-independent manner. For example, the stationary phase points are seen as intersections of Lagrangian manifolds. Some of the basics of this approach were presented in Aquilanti *et al* (2007). We have not specifically used the coherent state or any other representation.

Some aspects of this calculation carry through in an obvious way to higher spin networks, while for others nontrivial generalizations seem to be required. But we believe that an understanding of the $9j$ results are necessary for a full understanding of the asymptotics of higher spin networks.

We will report in more detail on the derivation of (1) in a later publication.

Acknowledgments

The authors would like to thank Enzo Aquilanti, Mauro Carfora, Annalisa Marzuoli and Carlo Rovelli for encouragement, many useful pieces of information, many stimulating conversations and much warm hospitality during the progress of this work. We would also like to thank Cynthia Vinzant for discussion of positive semidefinite completion, which helped greatly in proving that there are generically two admissible roots in the classically allowed region. This work was supported by a grant from the France–Berkeley Fund.

References

Alesci E, Bianchi E, Magliaro E and Perini C 2008 arXiv:0809.3718
Anderson R W, Aquilanti V and Ferreira C da S 2008 *J. Chem. Phys.* **129** 161101
Anderson R W, Aquilanti V and Marzuoli A 2009 *J. Phys. Chem.* A **113** 15106
Aquilanti V, Haggard H M, Littlejohn R G and Yu L 2007 *J. Phys. A: Math. Theor.* **40** 5637
Baez J C, Christensen J D and Egan G 2002 *Class. Quantum Grav.* **19** 6489
Barrett J W, Dowdall R J, Fairbairn W J, Gomes H and Hellmann F 2009 arXiv:0902.1170
Barrett J W and Steele C M 2003 *Class. Quantum Grav.* **20** 1341
Barrett J W and Williams R M 1999 *Adv. Theor. Math. Phys.* **3** 209
Berry M V 1976 *Adv. Phys.* **25** 1
Biedenharn L C and Louck J D 1981a *Angular Momentum in Quantum Physics* (Reading, MA: Addison-Wesley)
Biedenharn L C and Louck J D 1981b *The Racah–Wigner Algebra in Quantum Theory* (Reading, MA: Addison-Wesley)
Charles L 2008 arXiv:0806.1585
Conrady F and Freidel L 2008 *Phys. Rev.* D **78** 104023
de Gosson M 1997 *Maslov Classes, Metaplectic Representation and Lagrangian Quantization* (Berlin: Akademie Verlag)

Dupuis M and Livine E R 2009 *Phys. Rev.* D **80** 024035
Edmonds A R 1960 *Angular Momentum in Quantum Mechanics* (Princeton, NJ: Princeton University Press)
Freidel L and Louapre D 2003 *Class. Quantum Grav.* **20** 1267
Gurau R 2008 *Ann. Henri Poincaré* **9** 1413
Kapovich M and Millson J J 1996 *J. Differ. Geom.* **44** 479
Littlejohn R G and Yu L 2009 *J. Phys. Chem.* A **113** 14904
Marsden J E and Ratiu T 1999 *Introduction to Mechanics and Symmetry* (New York: Springer)
Marzuoli A and Rasetti M 2005 *Ann. Phys.* **318** 345
Maslov V P and Fedoriuk M V 1981 *Semi-Classical Approximation in Quantum Mechanics* (Dordrecht: Reidel)
Mishchenko A S, Shatalov V E and Sternin B Yu 1990 *Lagrangian Manifolds and the Maslov Operator* (Berlin: Springer)
Nomura M 1989 *J. Math. Phys.* **30** 2397
Ponzano G and Regge T 1968 *Spectroscopy and Group Theoretical Methods in Physics* ed F Bloch *et al* (Amsterdam: North-Holland) p 1
Ragni M, Bitencourt A C P, Ferreira C da S, Aquilanti V, Anderson R W and Littlejohn R G 2010 *Int. J. Quantum Chem.* **110** 731
Regge T 1961 *Nuovo Cimento* **19** 558
Regge T and Williams R M 2000 *J. Math. Phys.* **41** 3964
Roberts J 1999 *Geom. Topology* **3** 21
Schulten K and Gordon R G 1975a *J. Math. Phys.* **16** 1961
Schulten K and Gordon R G 1975b *J. Math. Phys.* **16** 1971
Taylor Y U and Woodward C T 2004 arXiv:0406.228
Taylor Y U and Woodward C T 2005 *Sel. Math. New Ser.* **11** 539
Trinkhaus H and Drepper F 1977 *J. Phys. A: Math. Gen.* **10** L11
Varshalovich D A, Moskalev A N and Khersonskii V K 1981 *Quantum Theory of Angular Momentum* (Singapore: World Scientific)
Wigner E P 1959 *Group Theory* (New York: Academic)
Williams R M and Tuckey P A 1992 *Class. Quantum Grav.* **9** 1409
Yutsis A P, Levinson I B and Vanagas V V 1962 *The Theory of Angular Momentum* (Jerusalem: Israel Program for Scientific Translations)